Journal of Catalysis 267 (2009) 5–13

Contents lists available at ScienceDirect

Journal of Catalysis

journal homepage: www.elsevier.com/locate/jcat

Influence of oxygen mobility on catalytic activity of La–Sr–Mn–O composites in the reaction of high temperature N_2O decomposition

D.V. Ivanov *, E.M. Sadovskaya, L.G. Pinaeva, L.A. Isupova

Boreskov Institute of Catalysis, Siberian Branch of the Russian Academy of Sciences, Pr. Acad. Lavrentieva 5, Novosibirsk 630090, Russia

ARTICLE INFO

Article history:
Received 29 April 2009
Revised 10 July 2009
Accepted 11 July 2009
Available online 26 August 2009

Keywords:
Lanthanum–strontium–manganese mixed oxide
Layer-structured perovskites
Oxygen diffusion
Oxygen vacancies
Nitrous oxide decomposition
Oxygen isotope exchange
SSITKA

ABSTRACT

Previous study suggested that either high oxygen mobility in layer-structured $(La_{1-y}Sr_y)_2MnO_4$ perovskite or high oxygen diffusion through intergrain boundaries is the reason why multiphase $La_{1-x}Sr_xMnO_3$ samples exhibit a high catalytic activity in high temperature N_2O decomposition. The absence of inhibiting effect of oxygen on the reaction rate for these samples allows us to suppose that surface segregation of layered perovskite increases oxygen mobility and facilitates oxygen desorption from the surface. In this paper, we aimed at determining the influence of surface composition on oxygen mobility and catalytic activity in high temperature N_2O decomposition. By means of steady-state isotopic transient kinetic analysis (SSITKA) the mechanism and kinetics of oxygen exchange were elucidated for three $La_{1-x}Sr_xMnO_3$ (x = 0, 0.3, and 0.5) samples considerably differing in phase composition and catalytic activity. The results obtained indicate that inactive single-phase $LaMnO_3$ exhibits both the lowest rate of oxygen exchange on the surface and the lowest rate of oxygen diffusion in the bulk. For $La_{0.3}Sr_{0.7}MnO_3$, the increased values of both rates as compared with $LaMnO_3$ can be interpreted as the appearance of a fast pathway of oxygen transfer through vacancies formed in the perovskite lattice to compensate the reduced cation charge. The highest values of the content of fast-exchangeable oxygen and oxygen diffusion coefficient were found for a multiphase sample containing layered perovskite, thus providing a strong correlation between oxygen mobility and catalytic activity in the reaction of nitrous oxide decomposition.

1. Introduction

Mixed oxides of the general formula $LaBO_3$ (B = Mn, Co, Fe, Cu, and Cr) constitute a broad class of materials including catalysts for many oxidative processes, membranes and cathodes for solid oxide fuel cells. An important feature of these materials is their ability to accommodate various ions of alkaline-earth metals into the La and B sublattices without noticeable changes in the overall bulk crystal structure. Substitution of foreign M^{2+} (M = Sr, Ca, and Ba) cations for La results in either the change of oxidation state of transition metal or the formation of anion defects in the packing of oxygen atoms. The formation of such defective structures influences oxygen mobility, and thus sometimes directly affects the catalytic properties of mixed oxides [1].

Among such mixed oxides, considerable attention has been focused on Sr-doped manganites as the promising catalysts for methane combustion. According to Marchetti and Forni [2], at low temperature (T < 700 °C) $La_{0.6}Sr_{0.4}MnO_3$ shows higher activity than non-modified manganite, which is due to the presence of weakly bound oxygen on the surface. On the other hand, Murwani et al. [3] consider that at temperatures above 300 °C the oxidizing agent is Mn^{4+}, which forms to compensate the charge change under Sr substitution for La. Ponce et al. [4] found as well that stability of Mn^{4+} ion seems to be the most important factor determining the catalytic activity of manganites in the oxidation of methane (200–800 °C). At high temperatures the catalytic activity depends on the lattice oxygen mobility [3,5]. As was shown by ^{18}O isotope exchange experiments, the last can be determined by either the structural properties of the samples, such as the presence of specific phase [6] and density of grain boundaries [7], or the oxidation state of Mn in Sr-doped manganites [3].

N_2O decomposition is another reaction that can be sensitive to oxygen mobility. According to the commonly accepted mechanism of this reaction [8]:

1. $N_2O + * \underset{k_{-1}}{\overset{k_1}{\leftrightarrow}} N_2O^*$;
2. $N_2O^* \overset{k_2}{\rightarrow} N_2 + O^*$;
3. $2O^* \underset{k_{-3}}{\overset{k_3}{\leftrightarrow}} O_2 + *$ (* is active site for N_2O adsorption).

Abbreviations: SSITKA, steady-state isotopic transient kinetic analysis; DDPA, differential dissolution phase analysis; XRD, X-ray diffraction; XPS, X-ray photoelectron spectroscopy.

* Corresponding author.
E-mail address: ivanov@catalysis.ru (D.V. Ivanov).

0021-9517/$ - see front matter © 2009 Elsevier Inc. All rights reserved.
doi:10.1016/j.jcat.2009.07.005

Nomenclature

D	diffusion coefficient of ^{18}O in the oxide bulk (m^2/s)
D_e	diffusion coefficient of molecular oxygen in catalyst pores (m^2/s)
D^{fast}	diffusion coefficient of fast-exchangeable ^{18}O in the bulk (m^2/s)
f_{34}	fraction of $^{16}O^{18}O$ in the gas phase
h	characteristic size of the oxide particle (m)
n	number of spherical layers of the catalyst's particle
N_g	quantity of oxygen atoms in the gas phase
N_s	quantity of oxygen atoms on the surface
N_{bulk}	quantity of oxygen atoms in the oxide bulk
N_{bulk1}	quantity of oxygen atoms in the first spherical layer
N_{bulk}^{fast}	quantity of fast-exchangeable ^{18}O atoms in the bulk (at./g)
N_{bulk}^{slow}	quantity of slow-exchangeable ^{18}O atoms in the bulk (at./g)
$N_{^{18}O^{16}O}$	quantity of $^{18}O^{16}O$ oxygen formed in the first 100 s of exchange (molec./g)
$N_{^{16}O_2}$	quantity of $^{16}O_2$ atoms released in the first 100 s of exchange (molec./g)
r	particle radius in spherical approach (m)
R	total rate of heteroexchange (s^{-1})
R^0	rate of homoexchange (s^{-1})
R^1	rate of heteroexchange between one oxygen atom from the gas phase oxygen and one oxygen atom from the solid (s^{-1})
R^2	rate of heteroexchange between molecular oxygen and two oxygen atoms of the solid (s^{-1})
S	surface area (m^2)
S_i	surface area of the ith spherical layer (m^2)
V	sample volume (m^3)
α_{bulki}	atomic fraction of ^{18}O in the ith spherical layer
α_{bulki}^{fast}	atomic fraction of fast-exchangeable ^{18}O in the ith spherical layer
α_g	atomic fraction of ^{18}O in the gas phase oxygen
α_s	atomic fraction of ^{18}O on the oxide surface
α_{Obulk}	atomic fraction of ^{18}O in the oxide bulk
β_i	coefficient of exchange in the ith spherical layer (s^{-1})
β_i^{fast}	coefficient of fast-oxygen exchange in the ith spherical layer (s^{-1})
β_{bulk}^{slow}	coefficient of slow-oxygen exchange in the bulk (s^{-1})
ξ	dimensionless reactor length
η	dimensionless depth of the oxide layer
τ	residence time (s)
τ_{bulk}	characteristic time of oxygen exchange in the bulk (s)
τ_{bulk}^{fast}	characteristic time of fast-oxygen exchange in the bulk (s)
τ_{bulk}^{slow}	characteristic time of slow-oxygen exchange in the bulk (s)
τ_{in}	characteristic time of oxygen molecule diffusion in catalyst pores (s)
τ_s	characteristic time of oxygen exchange on the surface (s)

Step 3 – desorption of oxygen – is most likely the rate-determining step, as was already observed for many catalysts [9,10].

In this case the correlation should exist between energy of activation for N_2O decomposition and surface-oxygen binding energy. Such correlation was found by Winter for a series of oxides at the temperature range 300–700 °C [11,12]. Moreover, Winter also relates the rate of N_2O decomposition to the lattice parameters of the oxide type such as the lattice spacing and the minimum O–O distance. However, it can be reasonably assumed that at higher temperatures other properties of oxides, e.g. bulk oxygen mobility, can become significant.

Earlier we investigated how the surface and phase composition of Sr-doped manganites $La_{1-x}Sr_xMnO_3$ ($x = 0$–1) influences their catalytic activity in the reaction of nitrous oxide decomposition at 900 °C. The multiphase samples containing $(La_{1-x}Sr_x)_2MnO_4$ with the K_2NiF_4-type structure exhibited the highest catalytic activity without reaction retardation by oxygen. This result lets us suppose that high activity of such systems could be due to both high oxygen mobility in the bulk of the solid and increased ratio between the rates of surface-oxygen desorption and adsorption.

Under this study, we aimed at examining the oxygen mobility–catalytic activity relationship for three samples of $La_{1-x}Sr_xMnO_3$ series ($x = 0$, 0.3, and 0.5), considerably differing in the catalytic activity in high temperature N_2O decomposition, by means of SSITKA [13–15].

2. Experimental

2.1. Catalysts preparation and characterization

The $La_{1-x}Sr_xMnO_3$ ($x = 0$, 0.3, and 0.5) catalysts were prepared by the organic polymerized complex method (Pechini route) [16]. Stoichiometric amounts of high purity metal nitrates [$La(NO_3)_3{\cdot}6H_2O$, $Mn(NO_3)_2{\cdot}6H_2O$, and $Sr(NO_3)_2$] were mixed in an aqueous solution. The solution was heated to 90 °C; 4 ml of water solution of citric acid (2 g/ml) and 3 ml of ethylene glycol were added while stirring. The solution was then evaporated to produce a viscous resin. Further heating (ca. 140 °C) resulted in decomposition of this viscous residue to form a perovskite precursor. The precursor was calcined in air at 900 °C for 4 h.

The samples were characterized by XRD in the as-prepared state and after the catalytic experiments using a URD-6 diffractometer with Cu Kα radiation. High-temperature diffraction experiments were performed on a Bruker D8 diffractometer using Anton Paar high-temperature X-ray chamber. The experiments were carried out in air and under vacuum (5×10^{-3} mbar) by heating the samples to 900 °C. Surface composition was studied by XPS using Al Kα irradiation. Detailed phase composition, cation ratio, and possible screening of one phase by another were analyzed by differential dissolution phase analysis (DDPA) [17].

2.2. SSITKA experiments

SSITKA is based on stepwise switches in the gas isotopic composition followed by continuous monitoring of differently labeled molecules. The installation used in this study consists of three main parts: gas flow control system, reactor block, and gas analysis system. The reactor is a 3 mm i.d. quartz tube located in a furnace. To control the temperature of the catalyst, a chromel–alumel thermocouple was installed outside the reactor, adjoining the catalyst bed. The experiments were performed as follows: the catalyst (0.025 g) was first treated in a mixture of 0.44 vol.% $^{16}O_2$/He flowing at a rate of 1.4 cm^3/s at 900 °C for 30 min; then the flow rate was raised to 16.7 cm^3/s. After 10 min of keeping in these conditions, the mixture was replaced stepwise by 0.44% $^{18}O_2$ in He at the same flow rate. In addition to $^{18}O_2$ this mixture also contained 1% of Ar. Argon response curve obtained after the replacement al-

lowed us to determine degree of approximation of mass transfer regime to plug-flow one. In our case Ar response curve behaves as a step function (presented below in all figures with the experimental data). Hence we suppose that the scrambling of the gas mixture passing through the catalyst bed can be excluded from the consideration. The outlet gas composition was analyzed by an on-line quadrupole mass spectrometer SRS QMS 200.

All SSITKA responses are analyzed as time variation of the fractions of differently labeled oxygen molecules: $f_{32}(t) = \frac{^{16}O_2}{\sum {}^{i}O{}^{j}O}$, $f_{34}(t) = \frac{^{16}O^{18}O}{\sum {}^{i}O{}^{j}O}$, and $f_{36}(t) = \frac{^{18}O_2}{\sum {}^{i}O{}^{j}O}$, where $\sum {}^{i}O{}^{j}O = {}^{16}O_2 + {}^{16}O^{18}O + {}^{18}O_2$.

The ^{18}O atomic fraction in the gas phase is calculated as follows:

$$\alpha_g(t) = \frac{{}^{16}O^{18}O + 2{}^{18}O_2}{2\sum {}^{i}O{}^{j}O}.$$

2.3. Catalytic activity tests

Catalytic activity in the reaction of nitrous oxide decomposition was studied using 3–20 mg of the catalyst (particles of 250–500 μm in size, 0.0325 cm^3 in volume) loaded in a quartz reactor of the same design as that used for the oxygen exchange experiments. The reactor operated at ambient pressure and 900 °C. The temperature was monitored by chromel–alumel thermocouple adjoining the catalyst bed. The gas mixture of 0.15 vol.% N_2O (+3 vol.% O_2) in He flowed across the catalyst bed at a rate of 16.7 cm^3/s (contact time 5×10^{-4} s). The outlet gas composition was analyzed by on-line gas chromatographs equipped with Porapak T column (i.d. = 3 mm, l = 3 m) to separate air and N_2O, and NaX column (i.d. = 3 mm, l = 2 m) to determine the concentrations of N_2 and O_2, which are the only reaction products.

3. Results and discussion

3.1. Samples characterization

According to the XRD data, the $LaMnO_3$ sample was a single-phase perovskite with orthorhombic cell (*Pnma* space group). In the $La_{0.7}Sr_{0.3}MnO_3$ and $La_{0.5}Sr_{0.5}MnO_3$ samples, a phase of $(La_{1-y}Sr_y)_2MnO_4$ with tetragonal K_2NiF_4-type structure (*P4/nmm* space group), consisting of alternate layers of $La_{1-x}Sr_xMnO_3$ and SrO, appeared in addition to Sr-substituted $La_{1-x}Sr_xMnO_3$ with pseudo-cubic structure (*Pm3m* space group). Structural parameters, phase composition and average particle size (calculated from XRD patterns and from BET surface area) are presented in Table 1.

For all the samples, particle size calculated using S_{BET} data (D_{BET}) was substantially greater than the X-ray particle size estimated by the Scherrer equation (D_{XRD}). This difference can be explained by the concretion of crystal domains forming the developed network of grain boundaries. As follows from the D_{XRD}/D_{BET} ratio, $LaMnO_3$ is characterized by the maximal density of grain boundaries among the studied $La_{1-x}Sr_xMnO_3$ samples.

To better understand the surface and phase composition of multiphase compounds, we studied them by differential dissolution phase analysis (DDPA). The results obtained indicate that $La_{0.7}Sr_{0.3}MnO_3$ is likely to be the solid solution of perovskite $La_{1-x}Sr_xMnO_3$ with a variable Sr content, which gradually decreases depthward in the bulk. The traces of $(La_{1-y}Sr_y)_2MnO_4$ are localized on the surface layers of the particles. Moreover, in the mixture of hydrochloric and nitric acid the trace quantity of X-ray amorphous MnO_x was detected. It would be expected to satisfy the overall sample stoichiometry.

For $La_{0.5}Sr_{0.5}MnO_3$ the surface is enriched with $(La_{1-y}Sr_y)_2MnO_4$ and easily soluble amorphous SrO_x, which partially screen the perovskite phase $La_{1-x}Sr_xMnO_3$. Further XPS analysis justified the surface enrichment with Sr and evidently indicated the presence of dispersed MnO_x. Formation of the $(La_{1-y}Sr_y)_2MnO_4$ phase and MnO_x on the surface of the particles could result from the partial decomposition of the Sr-supersaturated solid solution of perovskite [18].

According to XRD and DDPA in $La_{0.7}Sr_{0.3}MnO_3$, the amount of $(La_{1-y}Sr_y)_2MnO_4$ was negligible. As follows from high-temperature XRD, heating of this sample to 900 °C both in air and under vacuum led to the disappearance of $(La_{1-y}Sr_y)_2MnO_4$ phase probably due to incorporation into the perovskite lattice. Thus, in the conditions of oxygen exchange and catalytic activity experiments this sample was most likely a single-phase perovskite. For $La_{0.5}Sr_{0.5}MnO_3$ sample, heating to 900 °C both in air and under vacuum showed that the multiphase composition was stable.

3.2. Oxygen exchange

The results obtained when the isotopic composition of oxygen was switched from $^{16}O_2$ to $^{18}O_2$ in the gas mixture flowing over the $LaMnO_3$, $La_{0.7}Sr_{0.3}MnO_3$, and $La_{0.5}Sr_{0.5}MnO_3$ at 900 °C are shown as time variation of the $^{18}O^{16}O$, ^{18}O fraction (f_{34} and α_g, respectively), and argon (Fig. 1).

As indicated in Fig. 1, the greater is the degree of Sr substitution for La, the more pronounced is the delay between the $\alpha_g(t)$ and Ar responses. It definitely means that the overall rate of oxygen exchange for the multiphase sample is higher than that for the single-phase samples. However, $\alpha_g(t)$ transients cannot be expressed by a single-exponential function for each of the studied samples. This indicates that the time dependence of $\alpha_g(t)$ is at least a two-parametrized function including oxygen exchange on the surface and diffusion of labeled oxygen in the bulk of the solid.

According to [19,20], the higher is the rate of oxygen diffusion in the bulk, the smaller is the amount of $^{16}O^{18}O$ that will form at a close quantity of exchanged oxygen ($D \to \infty$, $f_{34}(t) \to 0$). Thus, for qualitative assessment of differences in the rate of oxygen diffusion in the bulk, the following coefficient was calculated:

Table 1
Structural parameters, phase composition, and average particle size (calculated from XRD and S_{BET} data) of $La_{1-x}Sr_xMnO_3$ samples (x = 0, 0.3, 0.5).

Sample	S_{BET} (m^2/g)	Phase composition	Lattice parameters (Å)			Space group	D_{XRD}[a] (nm)	D_{BET}[b] (nm)	h (μm)
			a	b	c				
$LaMnO_3$	2.8	$LaMnO_3$	5.486(2)	7.780(5)	5.492(2)	*Pnma*	90	320	0.16
$La_{0.7}Sr_{0.3}MnO_3$	4.1	$La_{1-x}Sr_xMnO_3$	3.875(1)			*Pm3m*	90	220	0.11
		$(La_{1-y}Sr_y)_2MnO_4$ (traces)							
		Two solid solutions of	3.888(2)			*Pm3m*	65		
$La_{0.5}Sr_{0.5}MnO_3$	5.5	$La_{1-x}Sr_xMnO_3$	3.866(2)			*Pm3m*		170	0.09
		$LaSrMnO_4$	3.857(4)		12.47(1)	*P4/nmm*	90		

[a] Crystal domain size calculated by Scherrer equation after correction for instrumental broadening.
[b] Equivalent cubic particle size calculated from BET surface area assuming density of $La_{1-x}Sr_xMnO_3$ equal to 6.67 g/cm^3.

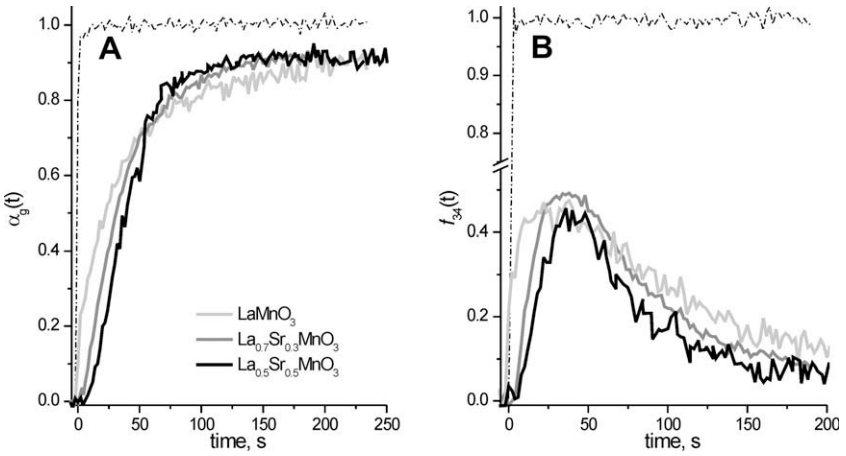

Fig. 1. The experimental $\alpha_g(t)$ (A) and $f_{34}(t)$ (B) responses observed for $LaMnO_3$, $La_{0.7}Sr_{0.3}MnO_3$, and $La_{0.5}Sr_{0.5}MnO_3$ at 900 °C.

$$\frac{N_{^{18}O^{16}O}}{N_{^{16}O_2}} = \frac{\int_0^{t_s} f_{34}(t)dt}{\int_0^{t_s} f_{32}(t)dt} \quad (t_s \approx 100\ \text{s}).$$

Time interval of 100 s after the isotope replacement was chosen to diminish miscalculation arising at integration of the tail parts of the curve, which are determined with lower accuracy. The calculated values of $\frac{N_{^{18}O^{16}O}}{N_{^{16}O_2}}$ are presented in Table 2.

As the calculations show, these values gradually decrease in the range $LaMnO_3 > La_{0.7}Sr_{0.3}MnO_3 > La_{0.5}Sr_{0.5}MnO_3$, which indicates that the substitution of Sr for La in manganites increases the lattice oxygen mobility.

Thus, two different steps that can control the overall rate of exchange are distinguished, i.e. oxygen exchange on the surface/subsurface layers of the catalyst and oxygen diffusion in the bulk. Oxygen mobility in the bulk obviously increases as La substitutes for Sr. To determine the kinetic parameters and exchange mechanism, we made numerical analysis of the isotope responses.

3.3. Model of isotope exchange

To make certain that the reaction of isotope exchange courses in a kinetic regime, a characteristic time of oxygen molecules diffusion in catalyst pores $\tau_{in} = \frac{h^2}{D_e}$ was estimated. Assuming that the catalyst particle has a spherical form, the characteristic size of the catalyst particle $h = 3V/S \approx 1.6 \times 10^{-7}$ m and $D_e \approx 10^{-3}$ m^2/s, the value of τ_{in} can be estimated as 10^{-10} s. This value certainly satisfies the criterion of the absence of transport limitation in catalyst particle under transient operation for step-response experiments [21]. Therefore, one can conclude that the dynamics of response is determined by the mechanism and the rate of oxygen exchange.

Three mechanisms of oxygen exchange between gas phase and the surface are distinguished [19,22,23]:

1. Homoexchange without participation of any oxygen atom of the oxide (characterized by the corresponding rate R^0):

$$^{16}O_{2(g)} + {}^{18}O_{2(g)} \leftrightarrow 2{}^{18}O^{16}O_{(g)}.$$

2. Simple heteroexchange between one oxygen atom of the gas phase oxygen and one oxygen atom from the structure of the solid (the corresponding rate R^1):

$$^{18}O^{18}O_{(g)} + {}^{16}O_{(s)} \leftrightarrow {}^{18}O^{16}O_{(g)} + {}^{18}O_{(s)},$$
$$^{18}O^{16}O_{(g)} + {}^{16}O_{(s)} \leftrightarrow {}^{16}O^{16}O_{(g)} + {}^{18}O_{(s)}.$$

3. Completely heteromolecular exchange between O_2 molecule and two oxygen atoms of the solid (the corresponding rate R^2):

$$^{18}O^{18}O_{(g)} + 2{}^{16}O_{(s)} \leftrightarrow {}^{16}O^{16}O_{(g)} + 2{}^{18}O_{(s)},$$
$$^{18}O^{16}O_{(g)} + 2{}^{18}O_{(s)} \leftrightarrow {}^{18}O^{18}O_{(g)} + {}^{18}O_{(s)} + {}^{16}O_{(s)},$$
$$^{18}O^{16}O_{(g)} + 2{}^{16}O_{(s)} \leftrightarrow {}^{16}O^{16}O_{(g)} + {}^{18}O_{(s)} + {}^{16}O_{(s)}.$$

The overall rate of heteroexchange is the only factor that determines the atomic fraction of ^{18}O in the gas phase, $\alpha_g(t)$. In turn, the atomic fraction of ^{18}O within the surface layers of the catalyst ($\alpha_s(t)$) depends on the rate of both heteroexchange on the oxide surface and isotope transfer in the bulk of catalyst.

For our system, the following scheme I of isotope exchange was proposed (Fig. 2).

The scheme comprises two main steps: (1) adsorption and exchange in the surface/subsurface layers, and (2) diffusion of labeled oxygen atoms in the bulk of oxide.

The isotope exchange between the gas phase oxygen and that in the oxide can be modeled for a plug-flow reactor using the following mass balance equations that describe the changes in the ^{18}O fraction [24–26]:
in the gas phase

$$N_g\left(\frac{\partial \alpha_g}{\partial t} + \frac{l}{\tau}\frac{\partial \alpha_g}{\partial \xi}\right) = -N_s R(\alpha_g - \alpha_s), \quad (1)$$

on the surface

Table 2
Calculated values of total amount of $^{16}O_2$ ($N_{^{16}O_2}$ – molec./g) and $^{18}O^{16}O$ ($N_{^{18}O^{16}O}$ – molec./g) taking part in oxygen exchange in the first 100 s and $\frac{N_{^{18}O^{16}O}}{N_{^{16}O_2}}$ coefficient.

Catalyst	Total amount of $^{18}O^{16}O$ formed during exchange (in the first 100 s) – $N_{^{18}O^{16}O}$ (molec./g)	Total amount of $^{16}O_2$ released during exchange (in the first 100 s) – $N_{^{16}O_2}$ (molec./g)	$\frac{N_{^{18}O^{16}O}}{N_{^{16}O_2}}$ (molec./molec.)
$LaMnO_3$	300×10^{19}	150×10^{19}	2
$La_{0.7}Sr_{0.3}MnO_3$	270×10^{19}	180×10^{19}	1.5
$La_{0.5}Sr_{0.5}MnO_3$	220×10^{19}	230×10^{19}	0.96

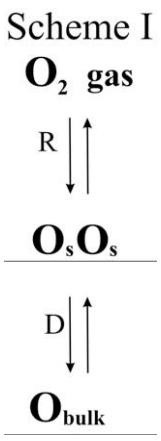

Fig. 2. A scheme I of the gas/surface(subsurface)/bulk oxygen exchange in the perovskite catalysts.

$$N_S\frac{\partial\alpha_s}{\partial t}=R(\alpha_g-\alpha_s)-S\frac{N_{bulk}}{V}\frac{D}{h}\left.\frac{\partial\alpha_{bulk}}{\partial\eta}\right|_{\eta=0}, \tag{2}$$

in the bulk of oxide

$$\frac{\partial\alpha_{Obulk}}{\partial t}=\frac{D}{h^2}\frac{\partial^2\alpha_{Obulk}}{\partial\eta^2}, \tag{3}$$

and supplemented with the equation describing changes in the $^{16}O^{18}O$ fraction:

$$N_g\left(\frac{\partial f_{34}}{\partial t}+\frac{1}{\tau}\frac{\partial f_{34}}{\partial\xi}\right)=N_s(R^0(2\alpha_g(1-\alpha_g)-f_{34})+R^1(\alpha_g(1-\alpha_s)+\alpha_s(1-\alpha_g)-f_{34})+R^2(2\alpha_s(1-\alpha_s)-f_{34})). \tag{4}$$

Initial and boundary conditions:

$$t=0,\quad \alpha_g=0,\quad f_{34}=0,\quad \alpha_s=0,\quad \alpha_{bulki}=0,$$

$$\xi=0,\quad \alpha_g=\alpha_g^{input},\quad f_{34}=f_{34}^{input}.$$

Here, α_g, α_s, and α_{Obulk} are the atomic fractions of ^{18}O in the gas phase oxygen, on the oxide surface and in the oxide bulk, respectively; f_{34} is the fraction of $^{16}O^{18}O$ in the gas phase; R^0, R^1, and R^2 are the rates of different types of exchange calculated per active site of the surface (s^{-1}); $R = 0.5R^1 + R^2$ is the total rate of heteroexchange (s^{-1}); D is the diffusion coefficient of ^{18}O in the oxide bulk ($m^2\ s^{-1}$); S is the surface area (m^2); V is the sample volume (m^3); h is a characteristic size of the oxide particle (m); η is a dimensionless depth of the oxide layer; τ is the residence time (s); ξ is a dimensionless reactor length; N_g, N_s, and N_{bulk} are the quantities of oxygen atoms in the gas phase, on the surface, and in the oxide bulk, respectively.

Quantities of oxygen atoms in the gas phase were known, while the quantities of oxygen atoms on the surface were taken to be equal to a monolayer (1×10^{19} at./m^2). The number of ^{18}O atoms capable of exchange N_{bulk}, the coefficient of diffusion in the oxide bulk D, and the rates of exchange R^0, R^1, and R^2 were estimated by modeling the isotope responses. Assuming that the shape of catalyst particle was close to spherical and the oxygen capable of exchange was distributed uniformly in the bulk, we divided the catalyst particle into n layers of equal volume and approximated the diffusion equation (3) by a set of n equations that describe the exchange between different spherical layers:

$$\frac{\partial\alpha_{bulk1}}{\partial t}=\beta_0(\alpha_s-\alpha_{bulk1})+\beta_1(\alpha_{bulk2}-\alpha_{bulk1}) \tag{5}$$

$$\frac{\partial\alpha_{bulki}}{\partial t}=\beta_{i-1}(\alpha_{bulki-1}-\alpha_{bulki})+\beta_i(\alpha_{bulki+1}-\alpha_{bulki})\quad(i=2,\ldots,n), \tag{6}$$

where α_{bulki} is the fraction of ^{18}O in the ith layer, β_i is the coefficient of exchange (s^{-1}) that varies with the surface of each layer, S_i:

$$\frac{\beta_i}{\beta_0}=\frac{S_i}{S}=\left(\frac{n-i}{n}\right)^{\frac{2}{3}}. \tag{7}$$

The ratio between diffusion coefficient and exchange coefficient β_0 is defined from the boundary conditions at $\eta = 0$:

$$S\frac{N_{bulk}}{V}\frac{D}{h}\left.\frac{\Delta\alpha_{bulk}}{\Delta\eta}\right|_{\eta=0}=N_{bulk1}\beta_0(\alpha_s-\alpha_{bulk1}). \tag{8}$$

Considering that within the frame of our spherical model of the particle (Fig. 3) $S = 4\pi r^2$,

$$V=4/3\pi r^3,\quad h=r,\quad \Delta\eta_1=\frac{1}{3n},\quad \frac{N_{bulk}}{N_{bulk1}}=n,$$

we obtain:

$$\frac{D}{r^2}=\beta_0(\Delta\eta_1)^2=\frac{\beta_0}{(3n)^2}. \tag{9}$$

If so, the exchange coefficients for each layer can be expressed in terms of diffusion coefficient:

$$\beta_i=\beta_0\left(\frac{n-i}{n}\right)^{\frac{2}{3}}=\frac{D}{r^2}(3n)^2\left(\frac{n-i}{n}\right)^{\frac{2}{3}}. \tag{10}$$

3.4. Numerical analysis of isotope responses

$LaMnO_3$. Fig. 4 presents the data on isotope fractions $\alpha_g(t)$ and $f_{34}(t)$ vs. time on stream measured in the SSITKA experiments over $LaMnO_3$ and calculated in accordance with the scheme I under the following ratios between the rate of heteroexchange on the surface and coefficient of labeled oxygen diffusion in the bulk:

- $R \gg D/r^2$ – the rate of oxygen diffusion in the bulk of the solid controls the overall rate of exchange.
- $D/r^2 \gg R$ – the rate of oxygen exchange on the surface controls the overall rate of exchange. In this case, $f_{34}(t)$ strongly depends on the type of oxygen exchange.

Calculated for the extreme case 1, $\alpha_g(t)$ response (Fig. 4a) fails to describe the break on the experimental $\alpha_g(t)$ curve observed in the time range around 40 s. So, in a period of 0–40 s the calculated values of $\alpha_g(t)$ exceeded the experimental values. It means that the rate of oxygen diffusion in the bulk of the catalyst was understated.

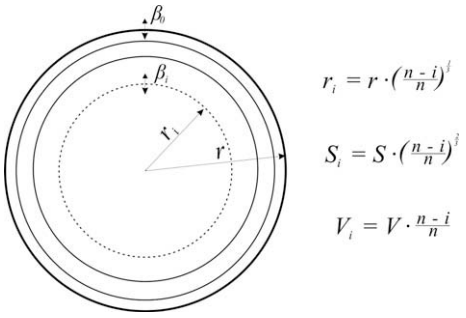

Fig. 3. A scheme of catalyst particle from a spherical approach.

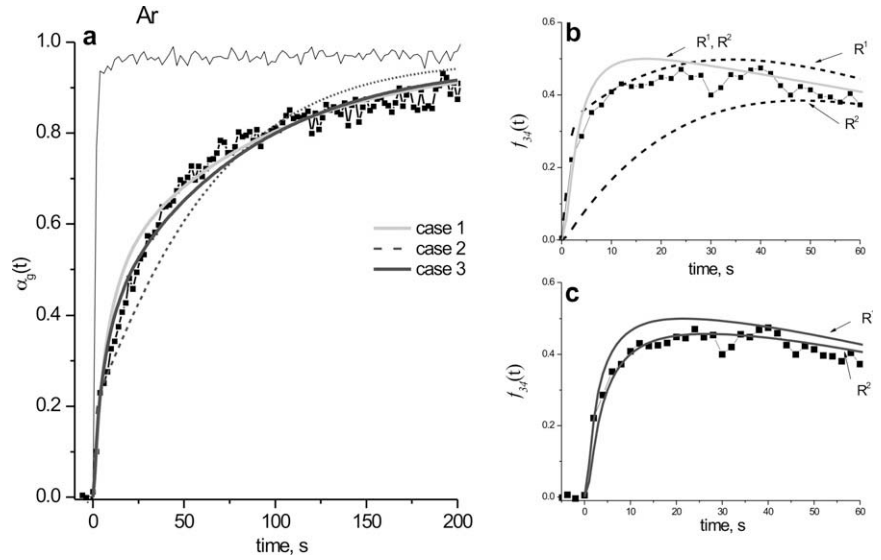

Fig. 4. Simulation responses $\alpha_g(t)$ (a) and $f_{34}(t)$ (b, c) over $LaMnO_3$. Point – experimental, lines – calculated by scheme I, cases 1–2 (a and b), case 3 (a and c). Curves R^1 and R^2 correspond to different mechanisms of heteroexchange.

However, attempts to increase the diffusion coefficient gave a worse fitting of the tail part of the curve. The calculated maximum of $f_{34}(t)$ is shifted to the short-time interval (5–25 s) irrespective of the mechanism of oxygen exchange on the surface (R^1 or R^2) (Fig. 4b).

Calculated for the extreme case 2, the values of R are evidently overestimated, and the time of relaxation is noticeably shorter than that observed for the experimental data. The calculated maximum of $f_{34}(t)$ is shifted to a longer time of stream (30–50 s), especially supposing R^2 mechanism (Fig. 4b).

As a result, the values of $\alpha_g(t)$ obtained for both extreme cases fail to fit the experimental data. It indicates that both oxygen exchange on the surface and diffusion in the bulk control the overall rate of oxygen exchange (case 3). In this case, in the initial period of time after the switch, oxygen exchange on the surface is the rate-determining step, while diffusion in the bulk becomes more significant with time. Table 3 lists the values of the oxygen exchange rate on the surface R and the diffusion coefficient D as well as the characteristic time of oxygen exchange on the surface and in the bulk (τ_s, τ_{bulk}).

Under the given values of the oxygen exchange rate on the surface, the distribution of isotope molecules $^{16}O^{18}O$ and $^{18}O_2$ at the outlet from the catalyst bed is approaching the equilibrium, and the difference between R^1 and R^2 mechanisms of exchange is partly suppressed. However, according to Fig. 4c, the mechanism R^2 provides more accurate description of $f_{34}(t)$ response, which is in agreement with the literature [27].

$La_{0.7}Sr_{0.3}MnO_3$. Numerical analysis of the $\alpha_g(t)$ and $f_{34}(t)$ dependences for $La_{0.7}Sr_{0.3}MnO_3$ sample (Fig. 5) indicates that with the same value of R obtained for $LaMnO_3$ sample we cannot achieve an appropriate fitting of experimental $\alpha_g(t)$ and $f_{34}(t)$ curves in the initial period of time (0–45 s), even by increasing the rate of oxygen diffusion in the bulk of the solid up to infinity (scheme I, case 1).

The maximum of calculated $f_{34}(t)$ curve is shifted to a longer time of stream, irrespective of the exchange mechanism (Fig. 5b). And vice versa, remaining unaltered the rate of oxygen diffusion in the bulk, we understate the overall rate of exchange in the time interval 5–50 s (Fig. 5a) even at extremely high value of R (scheme I, case 2).

Hence, for $La_{0.7}Sr_{0.3}MnO_3$ sample, both the rate of oxygen exchange on the surface and the rate of oxygen diffusion in the bulk have higher values than those found for $LaMnO_3$ sample. The best fitting of the experimental $\alpha_g(t)$ and $f_{34}(t)$ data can be achieved assuming that the bulk of the solid contains two different types of oxygen – O_{fast} and O_{slow} (scheme II, Fig. 6).

The first one is fast-exchangeable oxygen because of rapid diffusion in the bulk; the second one is slow-exchangeable lattice oxygen. We describe the fast exchange of oxygen by the same approximation of bulk oxygen diffusion (oxygen exchange between the spherical layers) as the one used for scheme I. We describe the slow exchange of oxygen by the exchange equations between O_{fast} and O_{slow} (scheme II, Fig. 6), which were added on the right-hand side of Eq. (6):

Table 3
Calculated values of oxygen exchange parameters for different La–Sr–Mn–O samples.

Catalyst	Exchange on the surface		Exchange in the bulk					
	R (s^{-1})[a]	τ_s (s)	N_{bulk} (at./g)		D (m^2/s)		τ_{bulk} (s)	
Model I – one type of bulk oxygen								
$LaMnO_3$	8	≈0.13	73×10^{20}		0.6×10^{-14}		≈60	
			N_{bulk}^{fast} (at./g)	D^{fast} (m^2/s)	τ_{bulk}^{fast} (s)	N_{bulk}^{slow} (at./g)	β_{bulk}^{slow} (s^{-1})	τ_{bulk}^{slow} (s)
Model II – two types of bulk oxygen								
$La_{0.7}Sr_{0.3}MnO_3$	15	≈0.07	35×10^{20}	2.3×10^{-14}	≈10	35×10^{20}	0.02	≈50
$La_{0.5}Sr_{0.5}MnO_3$	15	≈0.07	66×10^{20}	6.4×10^{-14}	≈4	17×10^{20}	0.02	≈50

[a] Supposing a concentration of active sites is 1×10^{19}.

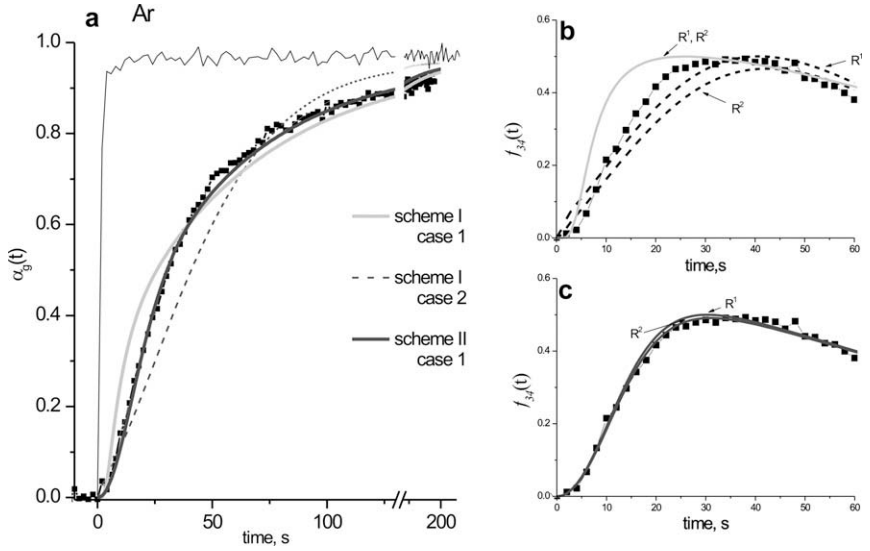

Fig. 5. Simulation responses $\alpha_g(t)$ (a) and $f_{34}(t)$ (b, c) over $La_{0.7}Sr_{0.3}MnO_3$. Point – experimental, lines – calculated by scheme I cases 1–2 (a and b) and scheme II case 1 (a and c). Curves R^1 and R^2 correspond to different mechanisms of heteroexchange.

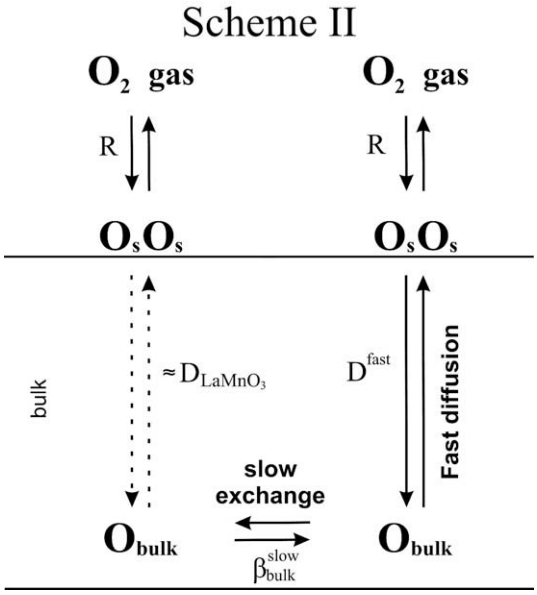

Fig. 6. A scheme II including two pathways of the gas/surface(subsurface)/bulk oxygen exchange.

$$\frac{\partial\alpha^{fast}_{bulki}}{\partial t} = \beta^{fast}_{i-1}\left(\alpha^{fast}_{bulki-1} - \alpha^{fast}_{bulki}\right) + \beta^{fast}_{i}\left(\alpha^{fast}_{bulki+1} - \alpha^{fast}_{bulki}\right) + \beta^{slow}\left(\alpha^{fast}_{bulki} - \alpha^{slow}_{bulk}\right) \quad (i = 2, \ldots, n), \tag{11}$$

$$\frac{\partial\alpha^{slow}_{bulk}}{\partial t} = \beta^{slow}\left(\frac{\sum\alpha^{fast}_{bulki}}{n} - \alpha^{slow}_{bulk}\right). \tag{12}$$

We assumed that the rate of exchange between the O_{fast} and O_{slow} as well as the quantity of O_{fast} and O_{slow} in each spherical layer was the same for each of the spherical layers. Finally, by modeling of isotope responses we determined the coefficient of fast-oxygen diffusion – D^{fast} (m^2/s), the quantity of fast-exchangeable ^{18}O atoms in the bulk (at./g) – N^{fast}_{bulk}, the coefficient of slow-oxygen exchange in the bulk (s^{-1}) – β^{slow}_{bulk} and the quantity of slow-exchangeable ^{18}O atoms in the bulk (at./g) – N^{slow}_{bulk}.

The best fit of the experimental data is reached by scheme II, case 1, provided that the amounts of fast- and slow-exchangeable oxygen, N^{fast}_{bulk} and N^{slow}_{bulk}, are in the ratio 1:1 (Fig. 5). As in the case of $LaMnO_3$ sample, the mechanisms of heteroexchange (R^1 and R^2) are indistinguishable. The total value of R, the diffusion coefficient of fast-exchangeable oxygen D^{fast}, and the coefficient of slow exchange with the lattice oxygen β^{slow}_{bulk} calculated for scheme II, case 1 as well as the characteristic time of oxygen exchange on the surface and in the bulk (τ_s, τ^{fast}_{bulk}, and τ^{slow}_{bulk}) are presented in Table 3.

$La_{0.5}Sr_{0.5}MnO_3$. For $La_{0.5}Sr_{0.5}MnO_3$ sample, experimental $\alpha_g(t)$ and $f_{34}(t)$ data cannot be well fitted by increasing only the value of R, while the other parameters of oxygen exchange (D^{fast} and the content of fast-exchangeable oxygen N^{fast}_{bulk}) obtained for $La_{0.7}Sr_{0.3}MnO_3$ sample remain unchanged (Fig. 7a and b; scheme II, case 1).

The best fit is achieved provided that both the rate of oxygen diffusion in the bulk D^{fast} and the content of fast-exchangeable oxygen N^{fast}_{bulk} for $La_{0.5}Sr_{0.5}MnO_3$ sample increase as compared with those obtained for $La_{0.7}Sr_{0.3}MnO_3$ sample (Fig. 7a and c; scheme II, case 2). As in the case of previous samples, the mechanisms of heteroexchange are indistinguishable. Table 3 lists out the parameters of exchange calculated in accordance with scheme II provided that the ratio between fast- and slow-exchangeable oxygen increases from 1:1 ($La_{0.7}Sr_{0.3}MnO_3$) to 4:1 ($La_{0.5}Sr_{0.5}MnO_3$).

3.5. Mechanism of oxygen transport in $La_{1-x}Sr_xMnO_3$

The results obtained by the numerical analysis of isotope responses indicate that the introduction of Sr into the perovskite lattice noticeably increases the coefficient of bulk oxygen diffusion. Moreover, two different types of oxygen – fast and slow exchangeable – need to be distinguished in the bulk of the catalyst to describe the observed responses. This means that in Sr-substituted samples the second faster pathway of isotope transfer in the bulk of the catalyst appears (Fig. 6).

The multiphase $La_{0.5}Sr_{0.5}MnO_3$ sample possessed the highest overall rate of oxygen exchange because of a greater contribution of the fast pathway to bulk oxygen diffusion compared to that found for $La_{0.7}Sr_{0.3}MnO_3$. In the general case, the appearance of these mobile oxygen species in $La_{1-x}Sr_xMnO_3$ can be due to the following reasons:

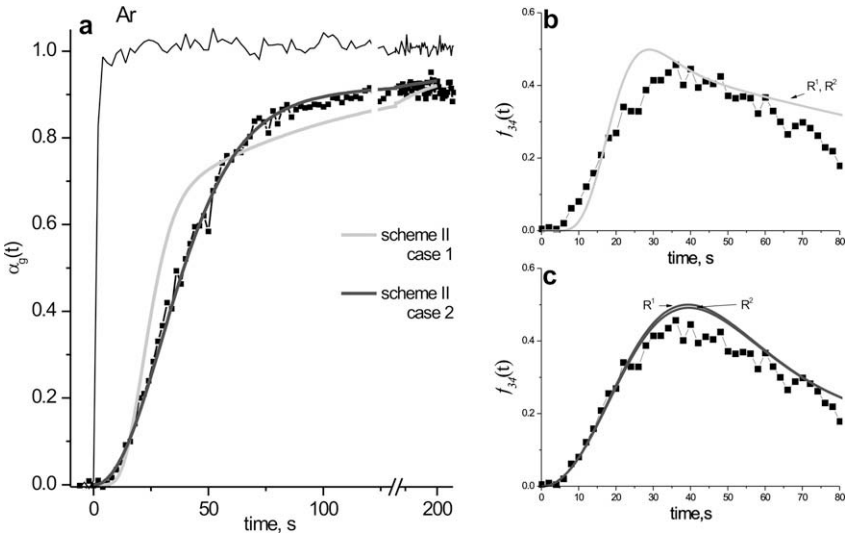

Fig. 7. Simulation responses $\alpha_g(t)$ (a) and $f_{34}(t)$ (b, c) over $La_{0.5}Sr_{0.5}MnO_3$. Point – experimental, lines – calculated by scheme II, case 1 (a and b) and scheme II, case 2 (a and c). Curves R^1 and R^2 correspond to different mechanisms of heteroexchange.

- formation of the highly developed network of grain boundaries. It is considered that oxygen diffusion along the grain boundaries is much faster than through the bulk [7,28];
- formation of the oxygen-deficient perovskite-like phases on the surface of the particles with high concentration of oxygen vacancies. This facilitates the oxygen diffusion via the vacancy mechanism [29,30];
- stabilization of highly dispersed manganese oxide on the sample surface. A more oxidized form of Mn oxides is characterized by high degree of oxygen lability, which can result in the formation of oxygen vacancies [31].

As regards the promoting effect of grain boundaries on oxygen mobility, clearly observed over $LaCo_{1-x}Fe_xO_3$ in the temperature range below 600 °C [7] and over $La_{0.8}Sr_{0.2}MnO_{3+\delta}$ at temperatures between 700 and 1000 °C [28], in our case the maximal density of grain boundaries was found for $LaMnO_3$, which is characterized by the lowest rate of oxygen mobility. However, since oxygen diffusion in the bulk of the solid is the rate-determining step of exchange, it is conceivable that diffusion of oxygen by grain boundaries can be sufficiently high.

One of the factors determining the high temperature oxygen mobility can be the formation of oxygen vacancies in the perovskite structure by the substitution of Sr for La. The concentration of oxygen vacancies depends on the degree of oxygen nonstoichiometry and changes as a function of temperature, partial oxygen pressure, and Sr-doping. Having studied the dependence of diffusion coefficients and thermodynamic enhancement factors on the partial pressure of oxygen in $La_{0.79}Sr_{0.2}MnO_{3-\delta}$, Belzner et al. [32] found that $La_{0.79}Sr_{0.2}MnO_{3-\delta}$ equilibrated in air to a composition with excess oxygen at temperatures below 760 °C and became oxygen deficient at temperatures above 815 °C. We also studied $La_{0.7}Sr_{0.3}MnO_3$ sample by high-temperature XRD and found that after cooling in vacuum from 900 °C to room temperature the lattice parameter was noticeably higher than that found for the initial sample. A higher value of the lattice parameter clearly indicates that during the heating to 900 °C removal of the weakly bound oxygen took place. Therefore, $La_{0.7}Sr_{0.3}MnO_3$ could become oxygen deficient in the conditions of oxygen exchange. Indeed, the emission of CO_2 and NO_x during the calcinations of perovskite precursor creates the reducing atmosphere favoring the formation of oxygen-deficient structures even at the preparation stage.

The oxygen-deficient perovskite decomposes as the content of Sr increases [18], thus resulting in a multiphase system that consists of Sr-enriched layer-structured phase $LaSrMnO_4$, and perovskite phase with a lower degree of Sr substitution for La–$La_{1-x}Sr_xMnO_3$ (the case of $La_{0.5}Sr_{0.5}MnO_3$). According to Taskin et al. [6], oxygen diffusion in the layer-structured phases can be by orders of magnitude higher than that in the simple doped perovskites. It can be due to the removal of oxygen atoms from lanthanide planes creating many oxygen vacancies for the oxygen motion. Indeed, Koudriashov et al. [6] found that for layer-structured phase $La_{1.5}Sr_{0.5}MnO_{3.99}$ the onset temperature of the oxygen out-diffusion was 150 K lower than for the perovskites. This indicates that the layered structure contains weakly bound oxygen, which can be easily removed.

Thus, the highest rate of oxygen diffusion obtained for the multiphase sample $La_{0.5}Sr_{0.5}MnO_3$ can be due to the presence of the layer-structured phase $LaSrMnO_4$ on the surface of the particles. However, based on the quantitative assessment of $LaSrMnO_4$ phase made by DDPA, the layer-structured phase can supply only 55% of fast-exchangeable oxygen. It means that the surface MnO_x and/or the $La_{1-x}Sr_xMnO_3$ phase localized in the bulk should make an additional contribution to the fast-oxygen exchange. As follows from the DDPA data, single-phase Sr-doped perovskite has the stoichiometric composition, $La_{0.78}Sr_{0.22}MnO_3$. $La_{0.7}Sr_{0.3}MnO_3$ also contains fast-exchangeable oxygen amounting to ca. 50%. Moreover, having studied the $La_{1-x}Sr_xMnO_3$ ($0 \leqslant x \leqslant 0.2$) by temperature-programed isotope exchange, Murwani et al. found that $La_{0.8}Sr_{0.2}MnO_3$ prepared by the citrate method exhibited the highest ^{18}O exchange activity [3]. Thus, the formation of oxygen vacancies in $La_{0.78}Sr_{0.22}MnO_3$ can also make a significant contribution to the fast-oxygen mobility in the bulk.

As for the contribution of MnO_x to high oxygen mobility in the multiphase $La_{0.5}Sr_{0.5}MnO_3$ sample, this question requires more detailed investigation.

3.6. Catalytic activity in N_2O decomposition

To clarify the effect of oxygen mobility on catalytic activity, we tested the studied samples in high-temperature nitrous oxide decomposition in the absence and in the presence of molecular oxygen in the gas mixture (Fig. 8).

The results obtained reveal a direct correlation between activity and oxygen mobility in the samples. So, less active undoped

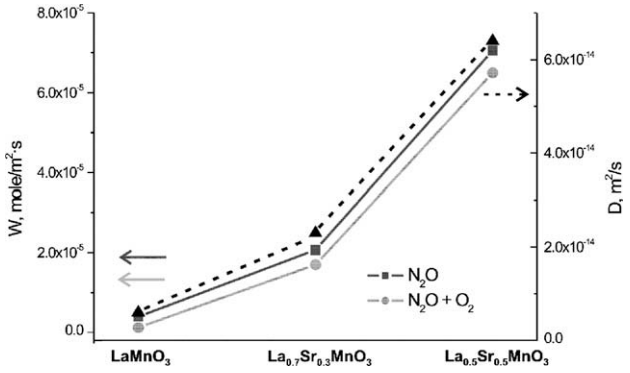

Fig. 8. A direct correlation between catalytic activity of the $La_{1-x}Sr_xMnO_3$ (x = 0, 0.3, and 0.5) samples in N_2O decomposition in the absence (■) or in the presence (●) of oxygen (900 °C, contact time 5×10^{-4} s) and the diffusion coefficient (▲).

$LaMnO_3$ has the lowest values of both the oxygen exchange rate on the surface and the coefficient of bulk oxygen diffusion. In $La_{0.7}Sr_{0.3}MnO_3$, the appearance of fast pathway of oxygen diffusion led to increased catalytic activity as compared with $LaMnO_3$. And finally, the multiphase $La_{0.5}Sr_{0.5}MnO_3$ shows the maximal oxygen mobility among the three studied samples and exhibits the reaction rate almost by an order of magnitude exceeding that found for $LaMnO_3$ and $La_{0.7}Sr_{0.3}MnO_3$ samples.

4. Summary and conclusions

The oxygen exchange behavior at high temperature in three samples of $La_{1-x}Sr_xMnO_3$ series (x = 0, 0.3, and 0.5) has been studied by a steady-state isotope transient kinetic analysis with a special emphasis on its relation to catalytic activity in high-temperature nitrous oxide decomposition. The results obtained indicate that the single-phase $LaMnO_3$ exhibits both the lowest rate of oxygen exchange on the surface and the lowest oxygen mobility in the bulk; this sample is also inactive. Sr promotion increases both the rate of oxygen diffusion in the bulk and the rate of oxygen exchange on the surface. This increase can be interpreted as appearance of the second faster pathway of oxygen transfer in the bulk of the catalyst through oxygen vacancies in perovskite structure. Appearance of the fast pathway of oxygen exchange in the bulk resulted in an increased catalytic activity as compared with $LaMnO_3$. The highest value of oxygen mobility in the bulk was found for the multiphase $La_{0.5}Sr_{0.5}MnO_3$ sample, the particles of which consist of Sr-doped perovskite phase covered with the $(La_{1-x}Sr_x)_2MnO_4$ phase of K_2NiF_4-type structure. For this sample, the content of fast-exchangeable oxygen attains 80% of the total amount of exchanged ^{18}O. This can be explained, first of all, by the structural features of the layer-structured $(La_{1-x}Sr_x)_2MnO_4$ phase with decreased oxygen bonding strength that favors the formation of disordered-free channels for oxygen motion in the lattice. Moreover, the formation of oxygen vacancies in simple Sr-doped perovskite located in the bulk of the particle can also make a significant contribution to fast-oxygen mobility in the bulk. As a result, the catalytic activity of this sample was almost by an order of magnitude higher than that found for $LaMnO_3$ and $La_{0.7}Sr_{0.3}MnO_3$ samples.

References

[1] H. Arai, T. Yamada, K. Eguchi, T. Seiyama, Appl. Catal. 26 (1986) 265–276.
[2] L. Marchetti, L. Forni, Appl. Catal. B: Environ. 15 (1998) 179–187.
[3] I.K. Murwani, S. Scheurell, M. Feist, E. Kemnitz, J. Therm. Anal. Cal. 69 (2002) 9–21.
[4] S. Ponce, M.A. Pena, J.L.G. Fierro, Appl. Catal. B: Environ. 24 (2000) 193–205.
[5] J.G. McCarty, H. Wise, Catal. Today 8 (1990) 231.
[6] I.A. Koudriashov, G.N. Mazo, I.K. Murwani, S. Scheurell, E. Kemnitz, J. Therm. Anal. Cal. 63 (2001) 59–68.
[7] S. Royer, D. Duprez, S. Kaliaguine, J. Catal. 234 (2005) 364–375.
[8] F. Kapteijn, J. Rodriguez-Mirasol, J. Moulijn, Appl. Catal. B: Environ. 9 (1996) 25–64.
[9] T.M. Miller, V.H. Grassian, Catal. Lett. 46 (1997) 213.
[10] J. Novakova, M. Lhotka, Z. Tvaruzkova, Z. Sobalik, Catal. Lett. 83 (2002) 215.
[11] E.R.S. Winter, J. Catal. 15 (1969) 144–152.
[12] E.R.S. Winter, J. Chem. Soc. A (1968) 2889.
[13] S.L. Shannon, J.G. Goodwin Jr., Chem. Rev. 95 (1995) 677–695.
[14] X. Zhang, P. Biloen, J. Catal. 98 (1986) 468–476.
[15] J. Nwalor, J. Goodwin Jr., P. Biloen, J. Catal. 17 (1989) 121–134.
[16] M.P. Pechini, US Patent No. 3,330,697, 1967.
[17] V.V. Malakhov, J. Mol. Catal. A 158 (2000) 143–148.
[18] M. Andrieux, C. Picard, J. Mater. Sci. Lett. 19 (2000) 695–697.
[19] V.S. Muzykantov, V.V. Popovsky, G.K. Boreskov, Kinet. Catal. 10 (1969) 1270.
[20] V.S. Muzykantov, V.V. Popovsky, G.K. Boreskov, Kinet. Catal. 14 (1973) 948.
[21] R.J. Berger, F. Kapteijn, J.A. Moulijn, G.B. Marin, J. De Wilde, M. Olea, De Chen, A. Holmen, L. Lietti, E. Tronconi, Y. Schuurman, Appl. Catal. A: Gen. 342 (2008) 3–28.
[22] V.S. Muzykantov, V.V. Popovsky, G.K. Boreskov, Kinet. Catal. 5 (1964) 624.
[23] K. Klier, J. Novakova, P. Jiru, J. Catal. 2 (1963) 479.
[24] J. Happel, E. Walter, Y. Lecourtier, J. Catal. 123 (1990) 12–20.
[25] E.M. Sadovskaya, Y.A. Ivanova, L.G. Pinaeva, G. Grasso, T.G. Kuznetsova, A. Veen, V.A. Sadykov, C. Mirodatos, J. Phys. Chem. A 111 (2007) 4498–4505.
[26] K. Klier, E. Kucera, J. Phys. Chem. Solids 27 (1966) 1087.
[27] C. Doornkamp, M. Clement, V. Ponec, J. Catal. 182 (1999) 390–399.
[28] R.A. De Souza, J.A. Kilner, J.F. Walker, Mater. Lett. 43 (2000) 43–52.
[29] A.A. Taskin, A.N. Lavrov, Yoichi Ando, Appl. Phys. Lett. 86 (2005) 0919110.
[30] S. Carter, A. Selcuk, R.J. Chater, J. Kajada, J.A. Kilner, B.C.H. Steele, Solid State Ionics 53–56 (1992) 597–605.
[31] T. Yamashita, A. Vannice, J. Catal. 161 (1996) 254–262.
[32] A. Belzner, T.M. Gur, R.A. Huggins, Solid State Ionics 57 (1992) 327–337.